Fatigue study of twisted polyamide sub-rope for floating wind turbines: Fast evaluation with heat build-up protocol and tomography study of mechanisms

Civier Laure [1, 2, 3], Chevillotte Yoan [1], Bain Cédric [1], Bles Guilhem [1], Damblans Guillaume [3], Davies Peter [2, 3], Marco Yann [1]

[1] UMR CNRS 6027, IRDL, ENSTA Bretagne, 2 Rue François Verny, Brest 29200, France
[2] IFREMER, Marine Structures Laboratory, 1625 Rte de Sainte-Anne, Plouzané 29280, France
[3] France Energies Marines, 525 Av. Alexis de Rochon, Plouzané 29280, France

Abstract :

Polyamide 6 fibre ropes are of interest for floating offshore wind turbine mooring lines but their fatigue durability represents a key aspect to characterize and validate on the new constructions and coatings developed for this long term application. This paper presents a fatigue study on laboratory scale polyamide 6 sub-ropes which were wetted before testing. A T-N curve describing ranges of [2%, 70%] of MBL and $[10^2, 10^5]$ is obtained. An investigation of the damage mechanisms, using X-ray tomography analysis and SEM images, is performed and highlights the complexity of the mechanical response of twisted ropes, due to their hierarchical multi-scale construction. Cyclic loading changes significantly the sub-rope aspect and architecture. Finally, this study describes the use of a heat build-up measurement protocol, for a rapid evaluation of the fatigue properties of ropes. The cyclic dissipated energy was determined from temperature measurements by an infrared camera. A first prediction using this method is proposed and shows that it could provide a powerful solution, to overcome the very long testing times required for fatigue studies on synthetic sub-ropes.

Highlights

► Extended S-N curve for a wet laboratory scale polyamide 6 sub-rope reaching 10^5 cycles. ► Investigation of the damage mechanisms using X-ray tomography analysis and SEM images. ► Use of a heat build-up measurement protocol for a rapid evaluation of the fatigue properties of ropes.

Keywords : polyamide 6, fatigue, synthetic rope, laid strand

1. Introduction

Offshore wind is well established in Europe with the largest operational wind farms for both fixed and floating foundation technologies [1]. There is currently 28 GW of grid connected capacity and 123 offshore windfarms in 12 European Countries. The target ambitions of the European Government are to deliver up to 160 GW of wind capacity by 2030 [1]. Offshore floating wind turbines will be located in exposed sites with significant environmental loading due to waves and wind. They will require mooring lines that maintain the floater position and withstand the environmental loads [2,3]. Synthetic fibre ropes have become extremely attractive as an alternative to steel chain and wire ropes due to their light weight, easier handling for installation and as they offer the possibility to reduce the overall footprint by using semi-taut to taut mooring arrangements. The high compliance and viscosity

of synthetic ropes will lower the line tension and provide damping. Polyester mooring lines could be used but they are too stiff for some conditions (strong swell and wind). Polyamide 6 (PA6) fibres are better-suited for this type of application in shallow water thanks to their low stiffness, good tensile strength and their viscous behaviour. The main limitation for the use of polyamide 6 ropes for mooring line is that their fatigue performances is yet to be confirmed. The response of a rope to fatigue loading is a combination of the responses at the different scales.

At the fibre scale, four failure modes have been observed on polyamide [4]:

- It may fail from internal hysteretic heating as polyamide has a large hysteresis loop (larger than polyester) and poor thermal conductivity.
- It may fail due to the permanent loading at the mean tension of the cyclic loading, hence showing a failure similar to a creep failure;
- It may fail due to crack initiation and propagation under tension;
- It may fail due to filament fatigue in tension-compression, in flexure or rotation.

Bunsell et al. [5] were the first to develop a machine able to perform load-controlled fatigue tests on fibres at high frequencies (50 Hz). This apparatus was then used in several fatigue test programs on Polyamide [6,7], Polyester [8,9] and higher stiffness fibres [10]. Using this test machine Bunsell et al. revealed a specific fatigue failure mechanism for polyamide fibres. It is characterized by a distinctive fracture morphology that they investigated using scanning electron microscopy. The creep failure mode is a fast crack propagation mainly in the radial direction. The fatigue mechanism happens in three steps: an initiation zone appears on the surface of the axis fibres; after a radial propagation, the crack deviates sharply and starts propagating along the fibre axial direction but with a penetration angle inside the fibre; finally, the cracks will propagate radially until the remaining section can no longer support the applied stress and a normal tensile fracture completes the break [5]. Herrera [11] study revealed the existence of a minimal load threshold, above which the failure is caused by the creep mechanism.

Beyond these basic mechanisms, two additional mechanisms are observed at the filament/fibre scales during rope scale tests:

- Creep, which is the elongation under a constant load of the rope construction and its constituent fibres or filaments.
- Fatigue, in tension-compression, in flexure or rotation.

Other mechanisms related to the multiscale nature of ropes must also be considered [12]:

- The hysteresis and internal heating within the rope and its constituents.
- Structural evolution during cycles due to the successive internal realignments of the rope structure.
- Internal abrasion between the sub-components of the rope at each scale (filaments, yarns, rope yarns and strands).

Previous studies showed that, at high loads, the creep rupture is dominant and that, at high or resonant frequencies, hysteresis will be dominant. Kenney et al. [4] performed fatigue tests characterized by cycling between a maximum load, ranging from 50%MBL to 95%MBL, and one-tenth of this value (load ratio of 0.1) and at a frequency of 1Hz. They obtained S-N fatigue plots for polyamide 6.6 single fibres, yarns and braided sub-ropes (in dry conditions). The fatigue resistance was shown to be nearly identical when plotted on a normalized S-N curve for the three different scales. Kenney et al. showed that creep rupture was the dominant mechanism in fatigue failure at all these scales. Hence, they suggested that the creep behaviour of a single fibre may determine the fatigue resistance

at each level of structure studied. They proposed a creep rupture model for the fatigue resistance based on the assumption that the creep rupture mode was dependent on the total time under load rather than on the number of cycles. The same conclusion was drawn by Mandell et al. (Mandell, 1987).

Additionally, Mandell et al. [13] showed that failures at lower loads and higher cycles usually occur by external or internal abrasion. Their work focused more on external abrasion and they proposed a model considering the loss of material to predict fatigue lifetime. 'External abrasion' was defined by the wear between the rope and the bollard at the termination region (eye-splice); 'internal abrasion' was defined by the wear between strands on inner and outer braids, in the splice or along the free part of the rope. Seo et al. [14] obtained yarn-on-yarn (YoY) abrasion data which indicated that, while polyamide 66 fibres showed better durability than polyester when dry, when tests were run wet, the polyamide 66 showed a significant reduction in wear resistance whereas polyester did not. They concluded that the coefficient of yarn friction is influential in structural rearrangements under tension. They highlighted the importance the coating can have on rope strength and fatigue durability as it prolongs the YoY wear life. Bain et al. [15] proposed an experimental evaluation of the main parameters influencing friction between polyamide fibres. They concluded that two parameters were controlling the friction coefficient between fibres: the inter-fibre angle and the friction angle.

The first studies presented [4,13,14] concluded that braided polyamide ropes had poor fatigue performance in comparison with polyester. Recent research suggests that an optimized rope architecture of polyamide rope and the use of appropriate internal coating allow fatigue lifetimes higher than the operation life of an offshore wind turbine to be reached [16,17]. Twisted polyamide 6 ropes with special coating have been shown to be good candidate. Banfield et al. [16] studied a twisted polyamide 6 rope characterized by a long lay-length and a new coating (marine finish) in wet conditions. They showed that fatigue results were greatly improved. In fact, improved coating and a longer lay-length will both reduce inter-strand abrasion, which has been shown to be the most critical mechanism in fatigue durability. Chevillotte [17,18] studied twisted polyamide 6 sub-ropes. In this study, fatigue tests and yarn on yarn tests performed in wet conditions. The yarn on yarn tests showed that a proper coating could increase the abrasion resistance. However, the fibre coating condition has to be controlled as it affects the fatigue performance. The fatigue tests on sub-ropes showed results that suggested polyamide ropes could have a fatigue durability close to that of polyester. More recently, to improve the confidence in polyamide 6 rope for mooring applications, Sorum et al. [19] analysed the performance of polyamide versus PET-fibre based rope. They performed experimental tests with complex loading to identify the parameters of the SYROPE model. They ran a fatigue damage analysis using a modelling approach. They showed that polyamide 6 lifetime could exceed polyester when used to moor the same floater in identical environmental loadings. This conclusion is not attributed to the material endurance but due to the mechanical properties which induce lower maximum load and cyclic amplitude of tension in using PA6 ropes. However, they propose a T-N curve only based on only one experimental point (made following the "thousand cycle load level test", TCLL) and mostly on numerical analysis.

The goal of the present study is to perform a complete study of the fatigue life of 3-stranded twisted polyamide sub-rope. It aims to obtain an extended T-N curve that reaches a reasonably high number of cycles to failure to improve the confidence in the fatigue lifetime of polyamide ropes. A specific sub-rope construction adapted to laboratory experiment is studied and allows a high number of cycles to be reached. Also, to improve our understanding of the damage mechanisms, X-ray tomography scans and SEM images are performed on a fatigued sample. Finally, the literature and the tests conducted in this study, showed that it is long, complicated and costly to determine the fatigue life of synthetic rope. Hence, this study also describes the use of a heat build-up measurement protocol to evaluate the fatigue properties of ropes rapidly [20–22]. An evaluation of the cyclic dissipated energy from the temperature measurements by an infrared camera is proposed. This heat-build up method

is performed on a laboratory scale sub-rope. A graphical approach based on the calculated dissipative energy allows a fatigue lifetime prediction to be obtained. It also provides an experimental approach that allows the relationship between the damage mechanisms and the maximum load and load ratio to be investigated.

2. Materials and methods

2.1. Materials

The synthetic rope studied is a reduced scale polyamide sub-rope for mooring lines supplied by Bexco, Hamme Belgium, specially manufactured for the research project. It was tested in the form of 1-meter-long (pin-to-pin) three-stranded rope samples with a diameter of around 11.5 mm, an MBL of 40 kN and a linear density of 90 000 tex (g/km); it will be referred to in this paper as '4Tsample'. Each strand is composed of yarns twisted together into rope-yarns. The rope-yarns are twisted together to form strands.

The yarns used were supplied by Nexis fibers and have a linear weight of 188 tex (g/km). A proprietary coating has been applied on the rope-yarns by the rope manufacturer Bexco. This coating aims to reduce the abrasion inside the rope improving its fatigue durability (the target fatigue lifetime for FOWT is 20 years) [17].
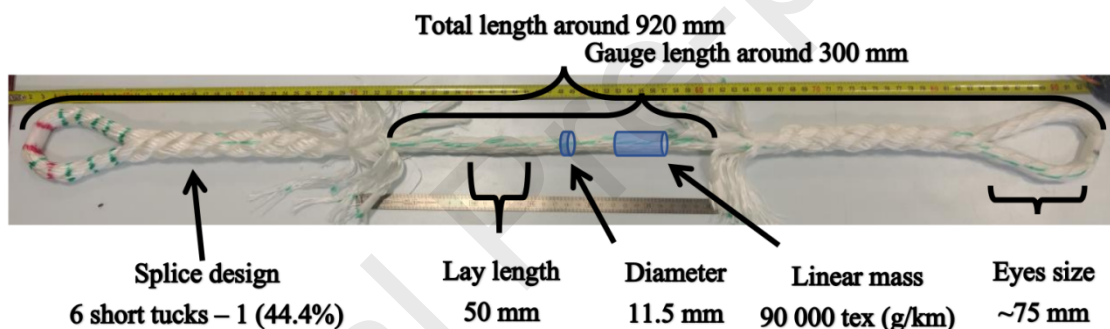
Figure 1 - 4T sub-rope sample with splices

This smaller scale is more adapted to laboratory experiments and the splices were prepared in the laboratory at ENSTA according to Bexco practice. This allowed more experiments to be performed as the cost was also reduced. Several rope samples were needed to develop and identify the parameters of a behavior law and to validate the model predictions.

An example of the 4T sub-rope samples is presented in Figure 1. All samples were terminated by eye splices in order to be connected to the tensile testing machine. The strand lay-length imposes the length of the splices.

Before each test, the sub-rope samples were fully immersed in tap water for 16 hours without load, in order to saturate them. An immersion time was estimated based on the work of Humeau *et al.* [23] on the same fiber type but without coating. During the tensile tests, the samples were maintained under water flow as explained in section 2.2. The soaking time is short but the small diameter of the fibres results in rapid saturation and the wetting continues throughout the test. For these tests, the use of tap water was preferable as seawater can damage the equipment. However, as the water serves mainly to keep the temperature down during cycling, no significant difference between tap water and seawater is considered.

2.2. Experimental procedure

The experimental requirements to perform fatigue tests, on synthetic fibre sub-ropes and ropes, are complicated. One difficulty is to control the failure zone in the gauge length using the right terminations. Splices are the most used as they allow the load distribution to be controlled and secure the failure in the gauge length. However, the splices must respect a minimum length with regards to the gauge length of the rope studied. Moreover, a minimum number of pitches must be present in the gauge length. These constraints result in long samples which require large test machines with long stroke. Also, the strain at rupture reached for polyamide 6 is around 20% which increases the minimum stroke required even more. The results at these scales are precious and hard to obtain.

A hydraulic machine developed for compression tests at high rates (Figure 2) called 'Servotest' allowed one-meter-long samples to be tested. This Servotest machine could also be used for quasi-static tensile tests, having a piston stroke of 600 mm. The maximum displacement rate is 100 mm.s^{-1} for quasi-static tests. The sample splices were linked to the machine by two 35-mm diameter loading pins.

Figure 2 - Servotest hydraulic machine used for testing

This is a vertical testing machine. As noted previously, the experimental tests should be performed in water (when possible). Following immersion in water for 16 hours, the samples were kept wet during the test by a system producing a constant and controlled vertical gravitational water flow around the sub-rope [17]. This consists of a volumetric pump with a low flow rate (around 1 litre.min^{-1}) that brings tap water near the top of the sample through a spiral-shaped pierced tube covered by a knitted fabric. This provides a homogeneous flow around the sub-rope section. The water then flows along the sample length by gravity. The lower loading pin was surrounded by a PVC tube to collect the sample water and return it to a tank. The HBM load cell has a range of ±50 kN and a resolution of 2 mV/V leading to a precision of around 10 N.

2.3. Bedding-in procedure

For industry station-keeping applications, a bedding-in process is performed to stabilize the properties of the rope. It consists of a procedure with a chosen sequence of loading to allow the permanent strain, due to construction modifications and reorientations of amorphous regions of fibers, to take place before the installation. Here a pre-loading sequence proposed specifically for the project is described in *Table 1*. It was applied with the loading rate equivalent to the ISO test.

Table 1 Bedding-in sequence performed before each test

Loading/unloading rate	Loading value [N/tex (%MBL)]	Creep/recovery duration [s]
$5 \cdot 10^{-4} s^{-1}$	0.07 (14)	3600
$-5 \cdot 10^{-4} s^{-1}$	0.01 (2)	3600

These two steps were applied for all tensile tests. The mechanical state at the end of this pre-loading is defined as the reference state for all strain measurements.

2.4 Heat build-up measurement protocol

The heat build-up measurement protocol is a fast method to evaluate the fatigue properties of materials [21,24]. An evaluation of the cyclic dissipated energy from the temperature measurements by an infrared camera allows for a prediction of the fatigue lifetime of a material. Chevillotte [17] first developed this technique on 4T sub-ropes and this study completes that work.

The heat build-up tests were performed on the Servotest testing device. To improve the self-heating measurement, the emissivity of the polyamide 6 rope has to be as close to 1 as possible, hence a black paint (Jelt® High temperature black paint) was applied to improve emissivity (Figure 3).

Figure 3 - 4T sub-rope sample with black paint on the gauge length to increase self-emissivity of the material

The sample was then immersed for 16 hours in a water tank. A High-Modulus Polyethylene (HMPE) fabric was wrapped around the eye-splices to avoid abrasion between the sub-rope eye-splice and the steel pin, hence avoiding a failure in the eye. The sample was then attached to the loading pins and the watering system described above was activated.

The environment affects thermal measurements; hence a custom plastic box was used in order to control the reflection conditions and to improve the thermal measurements. A sheet was also placed around the samples and the box (Figure 4). The self-heating measurements were performed using a Flir Systems infrared camera (reference Phoenix SC7600-BB). The integration time was set at 2000 µs. The thermal precision was evaluated around 40 mK.
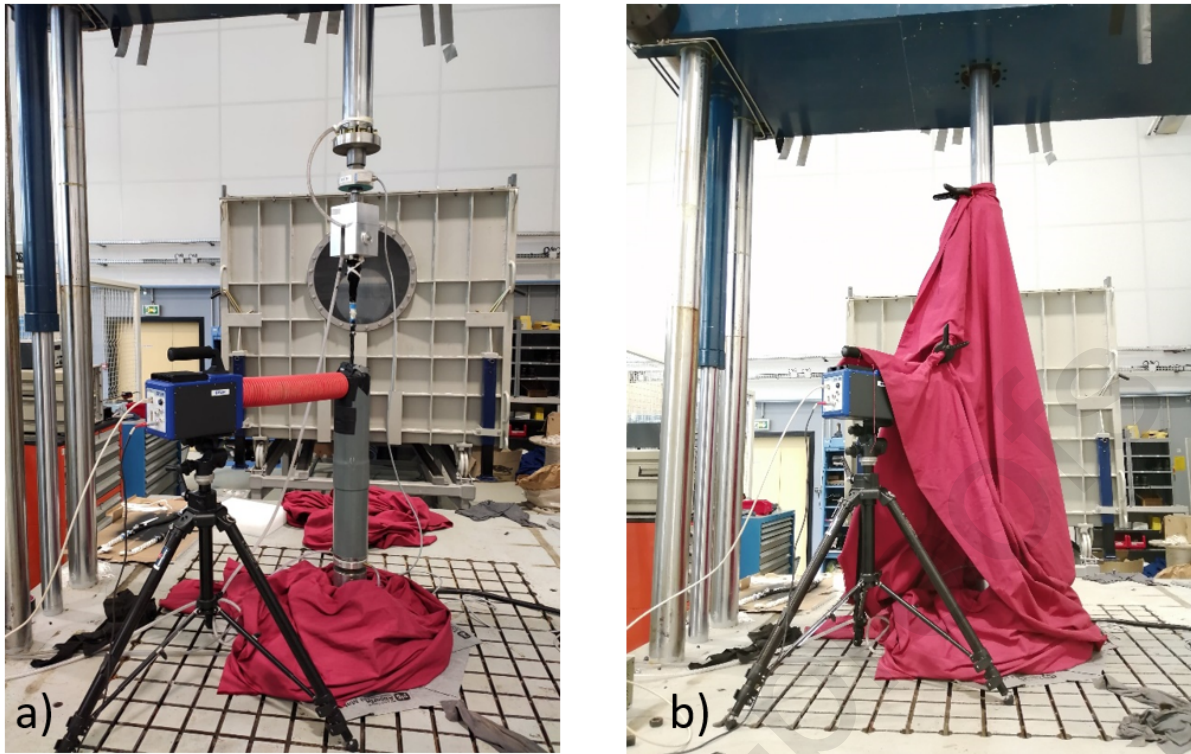
Figure 4 - Experimental set-up on the Servotest testing machine for fatigue test with self-heating measurement. a) plastic box and infrared camera installed. b) Sheet placed around the sample.

The bedding-in sequence was applied before each heat build-up test. The heat build-up test procedure consisted of several loading steps of 90 cycles, at 0.1 Hz, between 2% MBL (800N) and a chosen maximal tension level ranging from 20% to 70% of MBL (Figure 5). After each loading step, a load plateau, at the mean tension of the previous cycles, was held for 8 minutes to reach the stabilized state after cooling (Figure 5). The detailed procedures applied are described in Table 2.
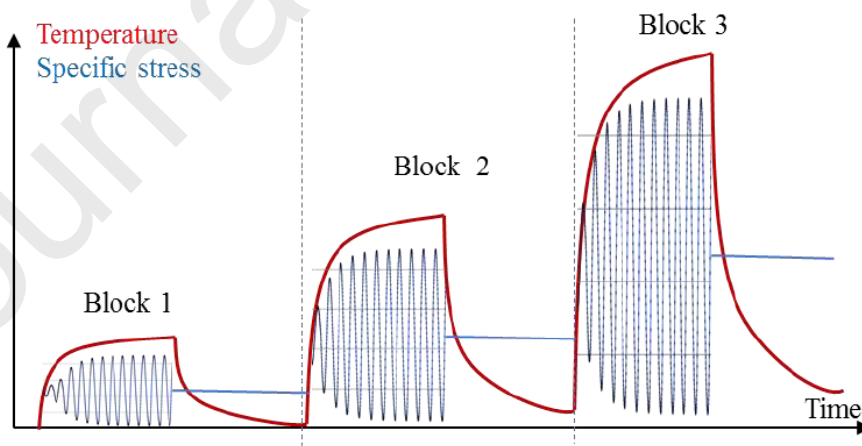
Figure 5 - Scheme of a self-heating test: Red curve: measured temperature evolution versus time. Blue curve: Specific stress evolution versus time

Table 2 - Loading sequences of cycle blocks for heat-build up on 4T sub-rope samples

Test Name	Self-heating blocks: maximal value (%MBL) during load step

7

1	20 – 25 – 30 – 40 – 45 – 50 – 55 – 60 – 65 – 67.5 – 70
2	20 – 20 - 25 – 25 – 30 – 30 – 40 – 40 – 45 – 45 – 50 – 50 – 60 – 60 – 70 – 70

The analysis of self-heating temperature, applied for this study, investigated the evolution of the dissipated energy, which is an intrinsic parameter. We considered a stationary state analysis [22] which allowed measurement of the thermal response of the full section of the ropes. The thermal evolution of the sub-rope sample and the surrounding box were recorded during the total duration of a loading step and a load plateau. An in-house developed software called Celenos® was used [25] to calculate the average temperature over the full rope diameter and the average temperature of the surrounding box. If necessary, the changes of the ambient temperature could be compensated. The increase of the temperature with time during the loading step is schematized in Figure 5 and can be identified as a saturating exponential function following Eq. 1:

$$T(t) = (\overline{\theta_{MAX}}) \times \left(1 - e^{-t/\tau_m}\right) \quad \textit{Eq. 1}$$

With $\overline{\theta_{MAX}}$ the maximal stabilized temperature, τ_m the characteristic thermal time during heating.

The evolution with time during the unloading and the plateau can be identified using Eq. 2 :

$$T(t) = \overline{\theta_{moy}} \times e^{-t/\tau_d} \quad \textit{Eq. 2}$$

With $\overline{\theta_{moy}}$ the mean stabilized temperature, τ_d the characteristic time during cooling.

Finally, the cyclic dissipated energy Δ^* is deduced according to Eq. 3:

$$\Delta^* = \left(\frac{\rho c \overline{\theta_{MAX}}}{f_r \tau_d}\right) \quad \textit{Eq. 3}$$

With ρ the density, c the specific heat capacity, f_r the frequency of the test.

2.5. Fatigue tests

The fatigue tests were performed on the Servotest testing device using the same experimental set-up as the heat build-up test described in section 2.4, with the watering system.

All fatigue tests were conducted with one self-heating measurement performed at the beginning of the test. The self-heating measurement set-up prevents strain measurements (a red sheet and a plastic box hide the sub-rope so no image correlation analysis can be performed).

The bedding-in sequence of 2 hours, presented in section 2.3, was performed before each fatigue test. For all the fatigue tests, the minimal tension level was kept fixed at 2% MBL (800N). The maximal tension level was modified, so the R ratio was not fixed for this fatigue campaign. The fatigue tests performed are described in Table 3 and were all performed at a frequency of 0.1 Hz. This frequency was chosen to be representative of the wave swell frequency met for the mooring application. The self-heating measurement was performed during the first 90 cycles (around 15 minutes) to be sure to reach the stationary state.

Table 3 - Fatigue tests performed during the study

Minimal tension level (%MBL - kN)	Maximal Tension level (%MBL – kN)	Ratio R
2 – 0.8	70 - 28	0.029
2 – 0.8	53 – 21.2	0.038
2 – 0.8	45 – 18	0.44
2 – 0.8	42 – 16.8	0.48
2 – 0.8	36 – 14.4	0.56
2 – 0.8	35 – 14	0.57
2 – 0.8	34 – 13.6	0.058
2 – 0.8	33 – 13.2	0.060
2 – 0.8	32 – 12.8	0.062
2 – 0.8	29 – 11.6	0.068
2 – 0.8	25 – 10.0	0.080

2.6. Scanning Electron Microscopy SEM

Scanning Electron Microscopy SEM (JEOL IT 300 LV) was used to assess the main phenomena involved in fatigue failure. The analysis was made in partial vacuum because polyamide is an electrical insulator. Hence, working in total vacuum will disturb the observation. On the contrary, working in partial vacuum allows to deviate the electrons beam and to decrease its power when interacting with the polyamide surface. The pressure in the chamber was 70 Pa. The detector used was a SED detector dedicated to scanning the surface electrons in partial vacuum. The voltage used was 10 kV, the working distance was 14.5mm.

2.7. X-Ray tomography observations

X-ray micro-tomography was used to examine both the details of the rope construction and the development of damage during cycling. This technique involves rotating a sample in an X-ray beam and recording the images. A 3-D reconstruction of the volume is performed with the recorded images. Figure 6-d) shows the equipment used (CRT Morlaix, France). The resolution was 20 µm. In order to scan a complete pitch length (50 mm), 3 scans with 2200 images were made. The total duration was 45 minutes. A specific experimental set-up (Figure 6-a, b, c) was developed to allow tomographic analysis on a sub-rope under a small tension (400 N). The attachments of the sub-rope consist of two dead turns around a pin. The sample is placed in a tube made of polyacetal to avoid disturbing the x-ray radiation. The sub-rope is mechanically loaded using mounting bolts. A load sensor placed at the bottom of the set-up allows the tension to be measured before putting it into the tomograph. After applying a tension, the sample was left in relaxation for 20 minutes (constant strain) to ensure a stabilization of the load value and of the construction.
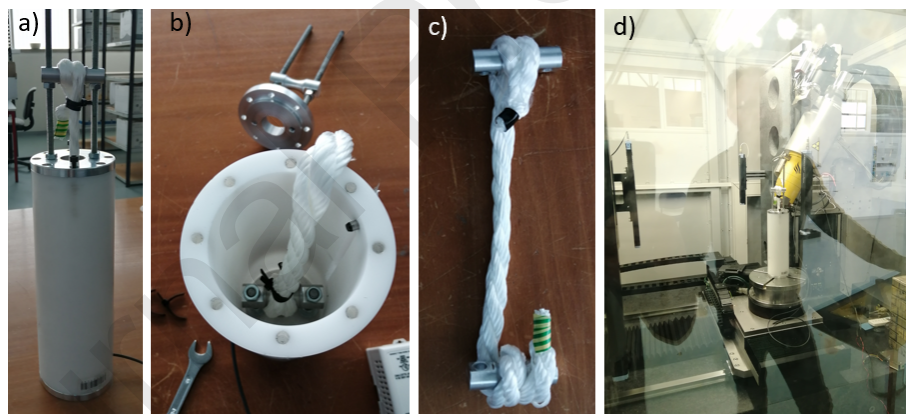
Figure 6 - Tomography set-up for 4T sub-rope. a) Whole set-up with sub-rope under tension. b) Set-up with sub-rope attached at the bottom. c) Example of the total attachment with dead turns. d) Set-up inside the X ray tomography chamber

3. Results and discussion

3.1. Extended T-N curve on 4T sub-rope

Twenty-one 4T sub-rope specimens were tested wet in fatigue by three different operators. The completed T-N curve with the maximal load (%MBL) plotted versus the number of cycles to failure is presented in Figure 7.
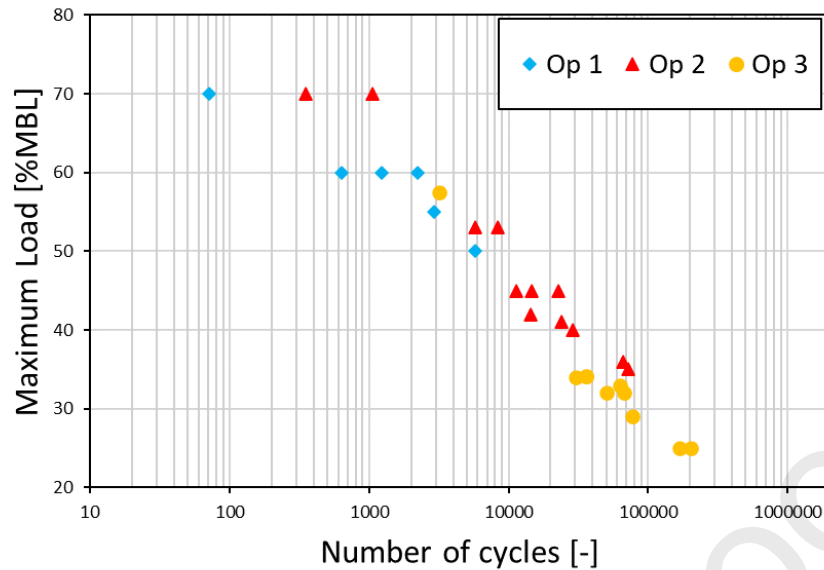
Figure 7 - Results of the fatigue tests on 4T sub-rope samples obtained by three different operators. Maximal load (%MBL) versus the number of cycles to failure

Eighteen specimens taken from the same batch of polyamide 6 sub-rope were tested (Op 1 blue diamonds and Op 2 red triangles) and nine specimens were tested from a new batch (Op 3 yellow circle markers). As a global conclusion, the twenty-one new fatigue test results confirm the linear trend observed and that no endurance plateau has been reached.

Figure 8 shows a summary of the results from all the fatigue tests on the 4T sub-rope scale and compares them to the results previously obtained on the 7T sub-rope sample [18], and to recently published results for two twisted constructions of polyamide 6 sub-ropes (large sub-rope construction with a MBL of 249 kN and small sub-rope construction with a MBL of 68 kN) by Banfield *et al.* [16]. The load range, normalized by the minimal breaking load (MBL) is plotted versus the number of cycles to failure. The experimental results for the 7T sub-rope samples are from fatigue tests performed with the same load ratio (cycling from 2% of MBL to a maximal value). The data from Banfield *et al.* are from fatigue tests to failure, conducted with a mean load of 40%MBL with load ranges between 70%MBL and 40%MBL (different load ratio). There are two results from Banfield 2017 obtained with two different constructions.
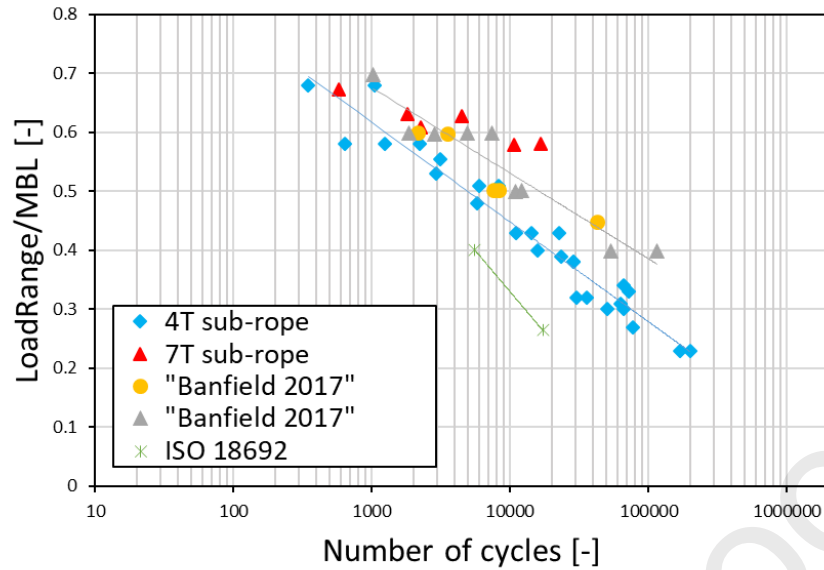
Figure 8 - Load range/MBL plotted versus number of cycles to failure. Comparison of the complete fatigue curve of 4T sub-rope samples obtained (blue diamond) to data obtained on 7T sub-rope sample (red triangles [18]) and to data obtained on two higher scale twisted polyamide constructions (orange circles and grey triangles [16]).

We chose to plot a semi-logarithmic scale because it illustrates well the differences in fatigue performances. Indeed, we often see data plotted on a log-log scale but it reduces the differences in fatigue lifetime between samples and might lead to incorrect conclusions. Also, using a log-log scale to propose a best fit can lead to an overestimation of the lifetime. Here, we will use the best fit of a classic power law (Eq. 4) to allow easier comparison with literature results.

$$K \cdot (LoadRange/MBL)^{-m} = N \quad \text{Eq. 4}$$

Where N is the number of cycles, LR is the load range, K is the intercept parameter of the curve and m the slope of the T-N curve. The parameters N and K obtained for the 4T sub-rope are presented in Table 4 and compared to other parameters from literature for polyamide and polyester.

Table 4 - Fatigue properties of the polyamide 4T sub-rope scale of this study, of polyamide rope from Banfield et al. [16], of polyester [26] of. The fibre rope properties are given for tension ranges normalized by MBL [16].

	PA6 4T sub-rope (this study)	PA6	PET
K	76	25.3	1.2×10^4
m	13.3	7.5	5.15

We observe the K values are significantly different for PA6 and PET (intercept of the curve). This is due to the shift between the T-N curves. Indeed, as observe in Banfield and Ridge study, PET is characterized by a higher fatigue lifetime and a T-N curve significantly shifted to the right and with a

lower slope. On Figure 8, we observe a slight shift of the 4T sub-rope data to the left compared to the 7T sub-rope, indicating a reduced fatigue lifetime. This is in accordance with the difference of construction between the samples. Indeed, the 4T sub-rope has a construction specifically made for laboratory experiments. It is characterized by a smaller number of components in the strands, rope-yarns and yarns as well as a higher twist angle (shorter lay-length). The twist angle will impact the amount of sliding of the strand during tensile loading and unloading, hence it will impact the inter-abrasion. On Figure 8, we observe an apparent difference for lower load ranges (from a load range of around 0.5 to 0.2) while the data at high load ranges, for the different specimens, seem to converge. This result could be interpreted by a change in the dominant failure mechanism for the 4T sub-rope samples. Mandell *et al.* [13] showed that creep is responsible for the fatigue failure at high loads while, at higher cycles and lower loads, inter-abrasion will dominate. The inter-abrasion mechanism is dependent on the construction of the rope. We can therefore expect to observe more differences in fatigue lifetime between samples with different constructions at lower loads. The fatigue tests performed on the 4T sub-ropes have a changing mean load. The points with a load range between 0.2 and 0.45 have a mean load between 11% MBL and 21%MBL while, the points with a load range between 0.5 and 0.7 have a mean load between 25%MBL and 45%MBL. For the lower mean loads, the inter-abrasion might be more active while for the higher mean loads, the creep will dominate, leading to a less significant impact of the lay length and construction on the failure. On the contrary, all the fatigue tests from Banfield *et al.* were carried out at a mean load of 40%MBL and only the load range is changing. Hence, for low ranges with 40%MBL mean load, we could suppose that the inter-abrasion is less active and the creep will dominate. That would explain the divergence of the fatigue lifetimes, at lower load ranges, between the 4T scale polyamide sub-rope and the polyamide sub-ropes from Banfield *et al.* on Figure 8.

Also, the splices are made manually for the 4T sub-rope and are of the minimal length required to perform a fatigue test. Longer splices would have secured the rupture in the gauge length and the load distribution. Indeed, Figure 9 shows the different types of failure obtained in this campaign for different samples. There are three types of failure: failure in the gauge length; failure in the splice (end); failure of one strand. The failure of only one strand was observed for the sample loaded with a maximal load of 25%MBL. This specific failure profile can be the result of inter-abrasion at lower loads. Inter-abrasion can lead to a loss of material associated with a non-uniform distribution of the stress inside the three strands. Hence, one strand might break first due a to stress concentration and reduced mechanical properties, but, as the load is not too high, the two other strands can continue to hold it without breaking. At higher loads, it also might be one strand that breaks first, but as the redistributed load is too high, the remaining strands will break immediately after the first one.

Figure 9 - 4T sub-rope samples after fatigue failure obtained during the MONAMOOR project

In comparison, the 7T sub-rope splices, tested by Chevillotte, were prepared by the supplier, with a higher length in comparison to the gauge length studied, and all failed between the splices. Hence, it

was expected that the 7T sub-rope would present a higher fatigue lifetime in comparison with the 4T sub-rope.

The difference observed between the 4T, the 7T and Banfield's 2017 results can be explained by differences in the construction and by differences in the coating. However, the 4T sub-rope construction is interesting as it provides a curve that is comparable to Banfield's result, that is conservative and that is easier to study in the laboratory.

The next section proposes a study of the damage mechanisms on 4T sub-rope samples after fatigue testing to investigate if some mechanisms can be identified.

3.2. Investigation of damage mechanisms

Figure 10 shows a rope after fatigue failure in the eye, which is interesting as we can observe its shape after fatigue as the gauge length was not broken. This picture reveals significant abrasion in the contact area between the rope strands. The inner surfaces in contact also reveal broken fibres. This first global observation requires some further analysis using dedicated experimental means.

Figure 10 - Damaged 4T sub-rope after fatigue testing

The internal abrasion, that is suggested to be the failure mechanism dominating at lower loads [13], is observed at the rope-yarn and strand scales. Tomography analysis can provide further insights on the damage mechanisms.

Oland *et al.* published a review of the condition monitoring techniques for synthetic fibre ropes and presented the computed X-ray tomography as one possible technology [27]. Davies *et al.* [28] performed X-ray tomography after a cyclic rope bending over a sheave (CBOS) test and they revealed that fibres had melted together during use which increased the rope's density. Also, Heinze and Michael [29] used tomography in-situ during a CBOS test and revealed internal abrasion associated with reduced rope diameter.

Hence, this section will present a study of the damage and failure mechanisms of 4T sub-ropes during fatigue testing, using optical microscopy, SEM and X-ray tomography analysis.

X-Ray tomography

The gauge length of a 4T sub-rope sample that broke in fatigue (cyclic loading between 2%MBL and 29%MBL) in the eye-splice has been analysed with X-ray tomography to investigate the damage mechanisms. A comparison of the tomography scans of this sample after fatigue with scans of a (non-wetted) virgin sample, is proposed. The two samples (virgin and after fatigue) are presented on Figure 11.

Figure 11 - Image of the samples analysed with X-ray tomography. a) Virgin sample. b) Sample after fatigue testing and failure in the eye-splice

Two scans were performed on each sample (virgin and after fatigue): one scan with no tension and one with a low tension of 300 N to observe a construction closer to a configuration during fatigue loading. Figure 12 and Figure 13 present the scans of the transverse section for the virgin and the fatigued sample respectively with tension and without tension; Figure 14 and Figure 15 present the tomography scans of the axial section of the virgin sample and after fatigue, respectively with tension and without tension. The blue lines on each image of the transverse section in Figure 12 delimit one strand (bigger outlines) and the red lines define one rope-yarn (smaller outlines) of the sub-rope. These allow the trajectory of these components along the sub-rope to be followed. Only one rope-yarn is indicated in Figure 13 for the scans under tension.
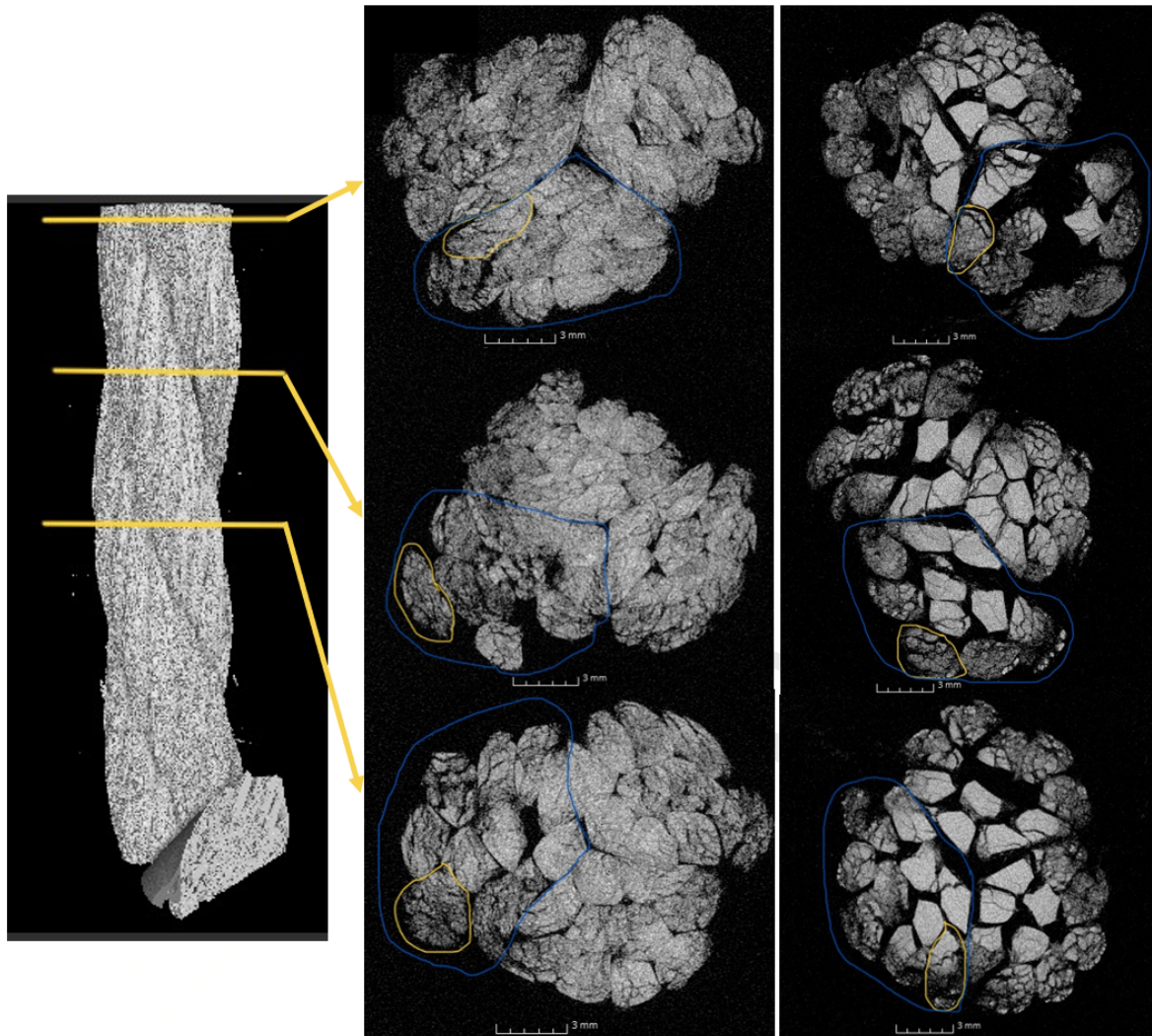
Figure 12 – Left: Tomography of a 4T sub-rope. Overview Right: Tomography scans of the transverse section of a 4T sub-rope without tension. Left: Virgin sample. Right: fatigued sample (after a fatigue test at 29%MBL). Yellow boundaries: rope-yarn. Blue boundaries: strand.

Several observations can be made on these tomography scans. First, we can appreciate the helicoidal trajectory of the strand along the sub-rope from scan to scan. In the same way, the helicoidal trajectory of a rope-yarn inside a strand can be followed. We observe that, depending on the position along the axial direction, the rope-yarns will alternate between being inside the sub-rope, in the contact region between strands, and outside the sub-rope. The rope-yarns will remain at the same radial distance from the helix axis of the strand. This is in agreement with the description of the twisted packing proposed by Leech [30].

The shape of the rope-yarns and strands is also consistent with the truncated wedges shape described by Leech for transversely soft components.

The angle between the rope-yarns and the helix axis changes along the radial direction. On the axial section scans (Figure 14 and Figure 15), the rope-yarn radial sections are not cut following the same angle. This is also in accordance with the description of Leech. Such a construction and trajectories will induce different loading conditions for a rope-yarn along its length. It will be subjected to more tension at the inner part of the sub-rope; in contrast it will go through more flexion and shearing when at the outer surface of the sub-rope.

16
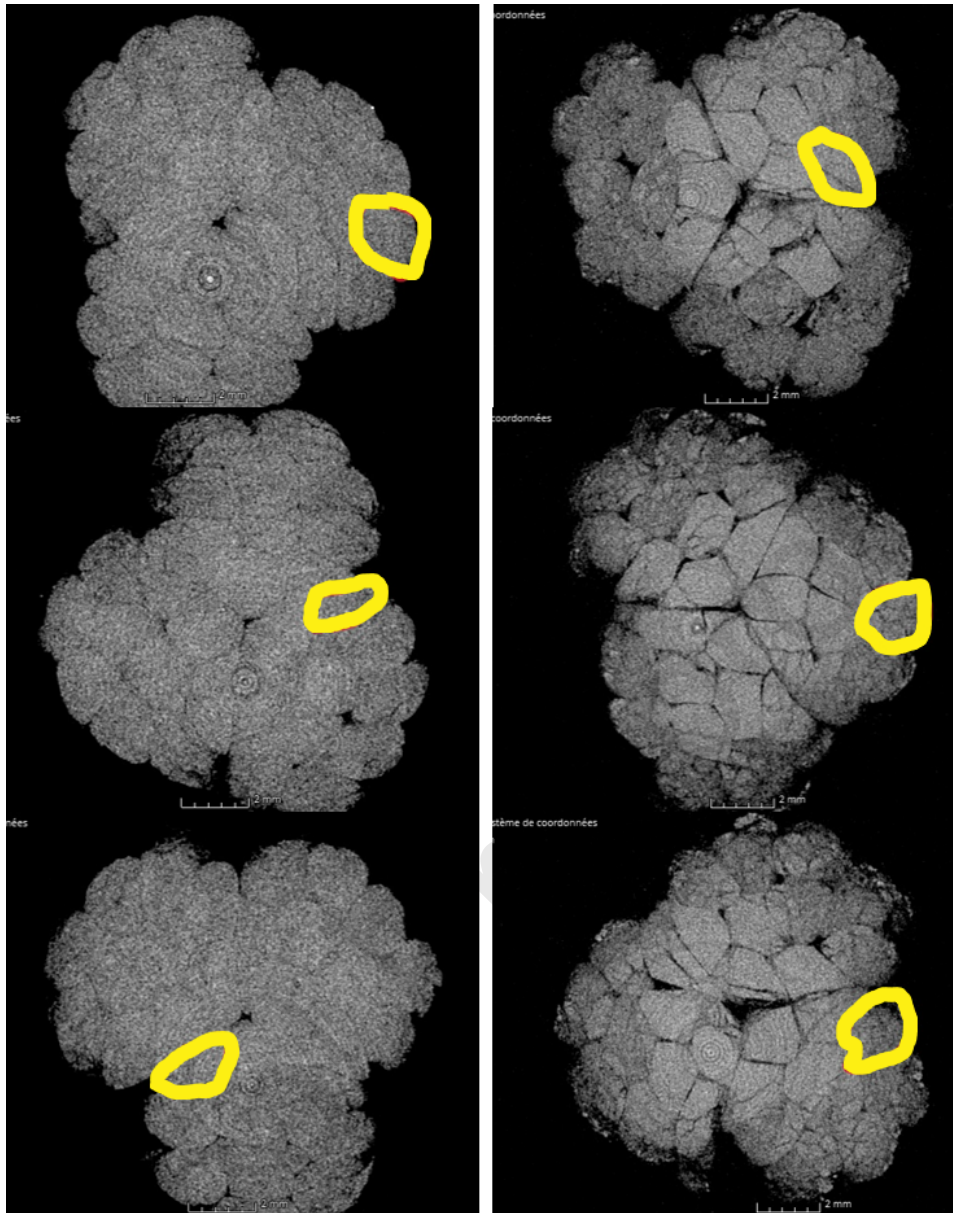
Figure 13 - Tomography scans of the transverse section of a 4T sub-rope under 300N tension. Left: Virgin sample. Right: fatigued sample (after a fatigue test at 29%MBL). Small red boundaries: rope-yarn.

Another interesting observation is a compaction of the rope-yarns is visible on the after-fatigue sample scans. On Figure 12 and Figure 13, at the inner surface of the after-fatigue sample, the rope-yarns are denser and more compact due to radial compression resulting in transverse compaction. Their shape is very angular both under tension but also without tension.

On Figure 13 and Figure 15, we also observe that the contact areas between the three strands, at 120°, are more visible on the fatigued sub-rope. These contact areas (inner surfaces) are subjected to radial compression and compaction that is associated with a change in the optical aspects of the contact area on the tomography scans. This difference between the fatigued and virgin sub-rope is even more visible in tension. In fact, it becomes difficult to detect the contact areas for the virgin sample whereas it is easy for the after-fatigue ones. Bain observed similar changes, due to lustering, in the contact area between HMPE textile ropes and a pulley ring [31,32]. Additional SEM scans were performed and are presented in the next section to investigate this phenomenon in more detail.
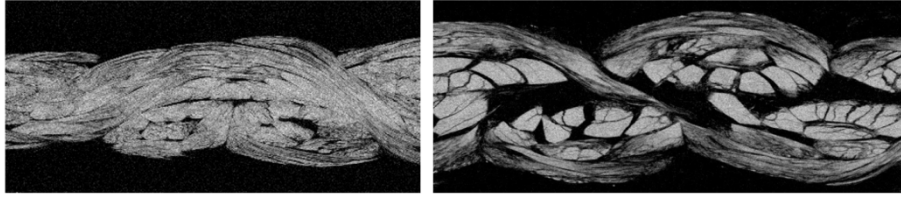
Figure 14 - Tomography scans of the axial section of a 4T sub-rope without tension. Left: Virgin sample. Right: fatigued sample (after a fatigue test at 29%MBL).
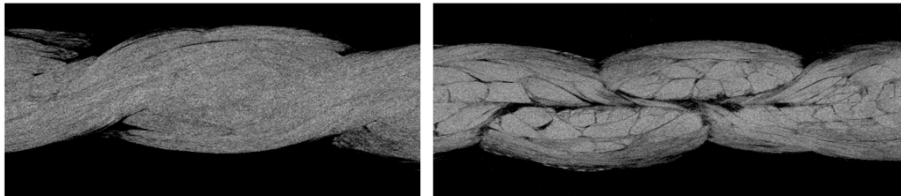
Figure 15 - Tomography scans of the axial section of a 4T sub-rope under 300N tension. Left: Virgin sample. Right: fatigued sample (after a fatigue test at 29%MBL).

Additional SEM analysis: study of the material at the filament scale

X-ray scans highlighted that the rope-yarns were more compact in the fatigued sample than in the virgin sample. Additional SEM observations were performed on the fatigued sample (Figure 11.b) after fatigue failure to investigate the state of the material at the filament scale. Figure 16 presents SEM pictures at different magnifications (left: virgin material and right: fatigued material). We observe the fibres composing the rope-yarns and yarns are more compacted for the fatigued sample. The new positioning and organisation of the fibres is associated with a smoother, more compact, and denser surface of contact, even without tension. No melting of fibres was observed; hence, the new state of the rope-yarns seems to only be due to the rearrangement of the fibres under tension. This new state of the surface at the contact area might induce a new friction coefficient:

- Either a lower friction coefficient due to the more compact arrangement and a hardening of the surface, and so, an improved fatigue durability. These observations are similar to the studies made by Bain on other textile fibres ropes [32].
- Or a higher friction coefficient as the study of Bain *et al.* [15] on the main parameters influencing the friction between polyamide 6 rope-yarns showed that the friction coefficient was higher when the fibres where parallel (longitudinal friction; friction angle of 0° between fibres).

Moreover, we observe on the fatigued sample, on Figure 16.b (magnification x50), a zone with marks that makes a specific angle with the fibre direction. This zone, highlighted on Figure 17, is suspected to be due to the friction of the fibres composing this strand with the fibres composing the other strand in contact with them.
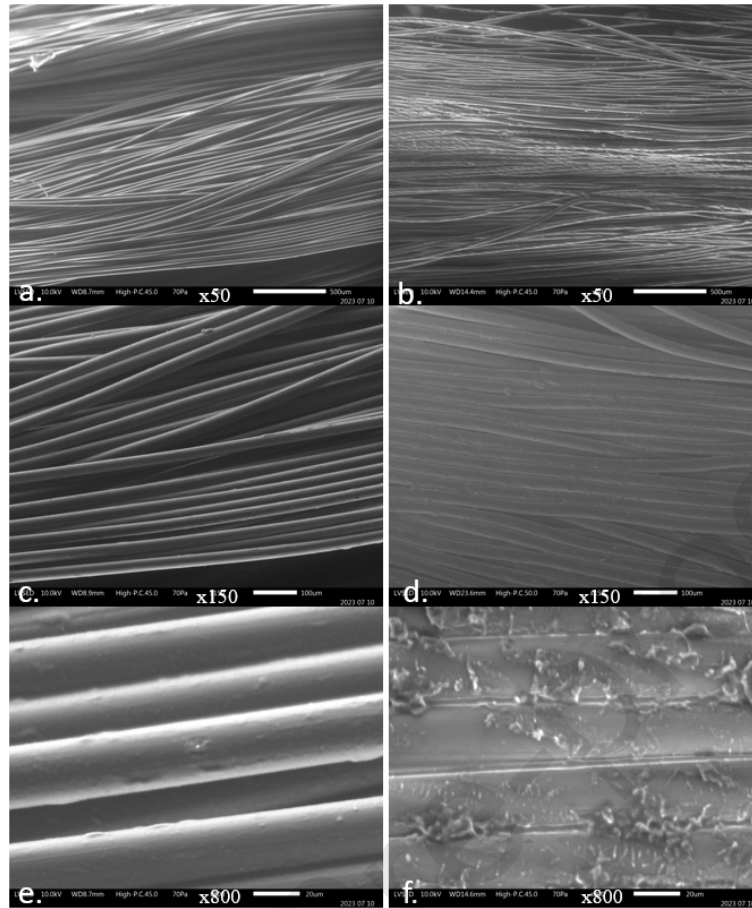
Figure 16 - SEM pictures: organisation of the material at the fibres scale for different magnifications: a) and b): x50. c) and d): x150 e) and f): x800. Left: virgin material. Right: Fatigued material

A zoom of this region was performed to allow better observation and is presented in Figure 17. This confirms that the surface aspect is similar to the marks made by the pull-out, or melting, of the material, or of the coating, during the contact and friction between the fibres. This highlights that the friction coefficient will depend on the orientation of the fibres with respect to the loading direction. The friction will cause a pull-out of the material under an angle different from the fibre axis. This will impact the friction coefficient between the fibres and probably the abrasion intensity as observed in the work of Bain *et al.* on the main parameters influencing the friction between polyamide rope-yarns that showed the friction coefficient was dependent on the angle between the fibres and the angle between friction sliding direction and fibre axis [15].
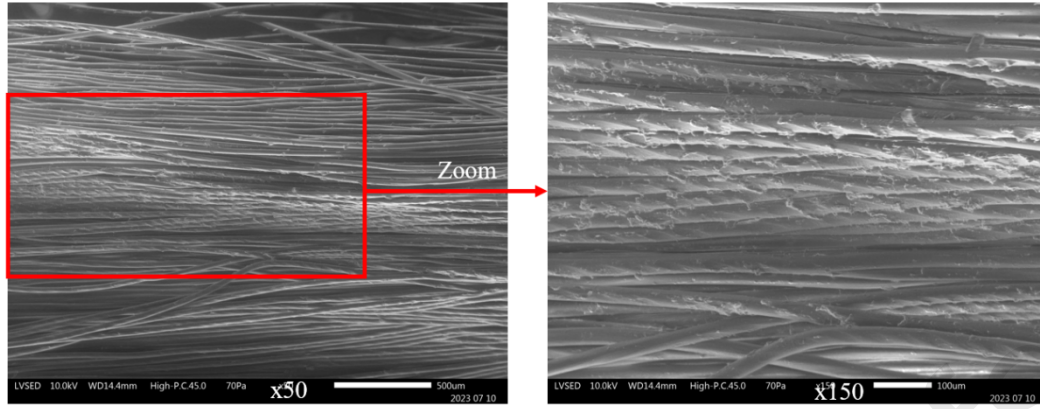
Figure 17 - Zoom of figure Figure 16-b). Magnification x150. Organization and aspect of the fibres.

3.5. Self-heating for fast fatigue prediction

The self-heating prediction method is based on the use of thermal measurements to determine the fatigue properties and to estimate lifetime of a material. A dissipated energy per cycle can be estimated from the thermal measurements and a heat built up curve, which describes the variation of the cyclic dissipated energy with the maximal load during the plateau, can be obtained. The analysis of this curve can give insights on the fatigue properties of the material. One example is the use of an energy criterion to predict the Wöhler curve. The method was developed on 4T sub-rope samples.

This study will, first, assess the repeatability and robustness of the self-heating experimental protocol on 4T sub-ropes when the operator changes. A self-heating prediction will be determined, based on the experimental campaign of self-heating tests. This prediction will be compared to the T-N curve obtained on 4T sub-rope.

Self-heating : hypothesis and method

This first section explains the method and the assumptions made to identify the thermal sources from the temperature measurements. The heat-equation can be written following Eq. 5 (Rosa & Risitano, 2000; Doudard et al., 2005; Jegou et al., 2013):

$$\rho c \dot{T} + div(\vec{q}) = \rho c S_t = \Delta + r + \rho T \cdot \frac{\partial^2 \Psi}{\partial v_k \partial T} \cdot \dot{V}_k + \rho T \cdot \frac{\partial^2 \Psi}{\partial \varepsilon^e \partial T} \cdot \dot{\varepsilon}^e \qquad \text{Eq. 5}$$

With ρ the density, c the specific heat capacity considering the internal variables V_k as constant, T the temperature, $\vec{q}$ the heat flow vector, S_t the thermal sources, Δ the intrinsic dissipation, r the external heat supply, Ψ the Helmholtz free energy and ε^e the elastic strain tensor.

Some classical hypotheses can be applied: first the external heat sources are supposed not to be time-dependent; then the temperature ranges are supposed to be low enough (estimated to be below 10°C according to study on 7T sub-rope samples), hence, we can neglect the variations of ρc and the couplings between the temperature and the internal variables ($\dot{V}_k$). We define λ the conductivity tensor. Using Fourier's law, the heat equation in Eq. 5 can be written:

20

$$\rho c \dot{T} \; - \; \lambda \Delta T = \Delta + \rho T \cdot \frac{\partial^2 \Psi}{\partial \varepsilon^e \partial T} \cdot \dot{\varepsilon}^e \qquad \text{Eq. 6}$$

We consider only cyclic tests in this study. During such tests, the external heat supply is supposed equal to zero and the thermo-elastic term cancels out over a mechanical cycle. We define the mean temperature variation θ ($= T - T_0$). Hence, solving the heat equation reduces to Eq. 7:

$$\rho c \dot{\theta} \; - \; \lambda \Delta \theta = \Delta \qquad \text{Eq. 7}$$

It is convenient to use the intrinsic dissipation over a cycle Δ^* and the frequency f_r to express the heat equation as:

$$\rho c \dot{\theta} \; - \; \lambda \theta = \; \Delta^* \cdot f_r \qquad \text{Eq. 8}$$

Our sub-rope sample is a multi-scale material and the dissipation field is likely to be heterogenous. However, consistent with the fact that the stress and the strain are averaged, we consider an average temperature over our sample. The thermal measurements made during this study are represented on Figure 18:
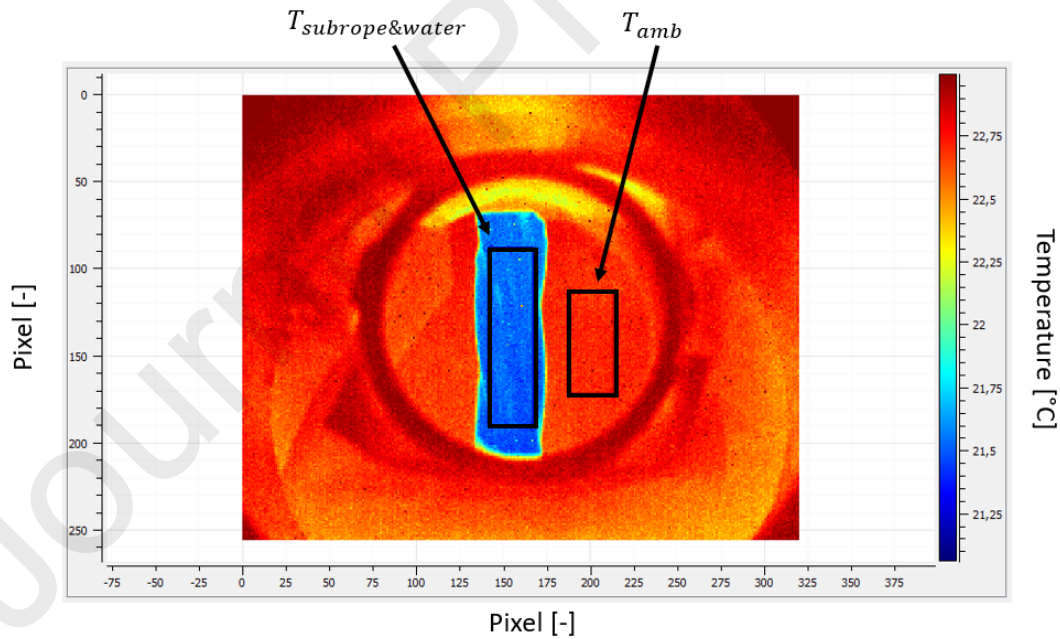
Figure 18 - Temperature map obtained from infrared radiation measurements during a self-heating test. The blue part is the sub-rope. "T_subrope&water" is the temperature measured from the infrared radiation of both the rope and the water trickle; "T_amb" is the ambient temperature surrounding the sub-rope and water trickle.

The mean temperature variation is measured on one zone of the sub-rope. A measurement of the ambient temperature is also performed to correct the temperature drift due to the environment (T_{amb} in Figure 18). Experimentally, the infrared camera measures a flux of infrared radiations. A

radiation balance is applied and we convert the measured radiations into temperatures. In a first approximation, we did not correct the impact of water on the radiation balance.

As we did not correct for the water in the radiation balance, we are not measuring the temperature of the sub-rope but of the sub-rope and of the water surrounding it. Hence, we could not calculate the intrinsic dissipation of the sub-rope. However, we can assume that the total measured dissipation will be related to the intrinsic dissipation of the sub-rope. For simplicity, we will note Δ^*, the global dissipation per cycle (without removing the water contribution to the radiation balance).

Under this assumption, it can be written that:

$$\dot{\theta} - \frac{\theta}{\tau_{eq}} = \frac{\Delta^* \cdot f_r}{\rho c} \quad \textit{Eq. 9}$$

With τ_{eq} the characteristic thermal time which is dependent on the thermal boundary conditions and the sample geometry and $\frac{\theta}{\tau_{eq}}$ representing the heat loss of the sub-rope, and water, with the environment. To calculate the equivalent dissipation from the average temperature, we have to determine the characteristic thermal time. Figure 19 is a plot of the temperature versus time during one block of self-heating.
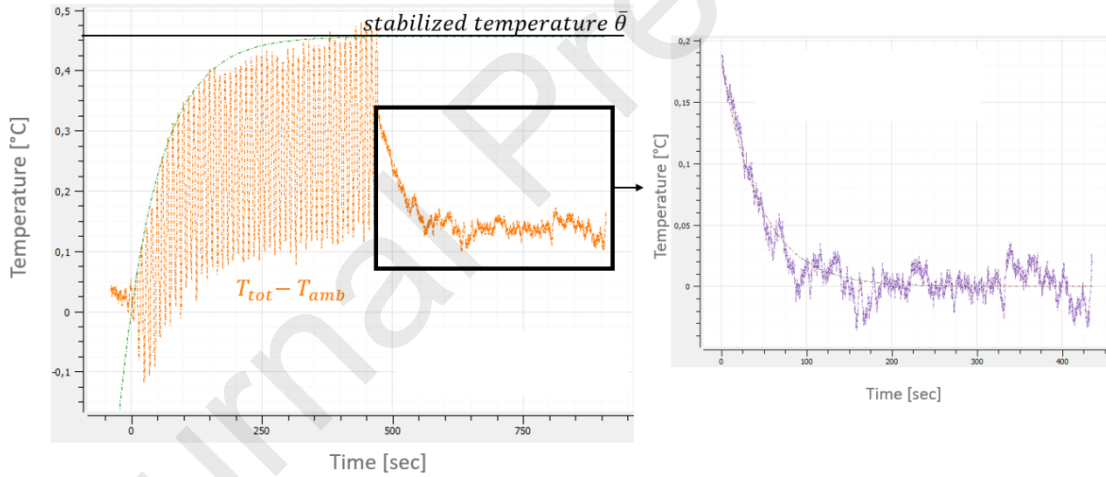
Figure 19 - Average temperature [°C] versus time [sec] during one block of self-heating. Method to identify $\boldsymbol{\tau_{eq}}$ and $\overline{\boldsymbol{\theta_{MAX}}}$ using Eq. 1 and Eq. 2

The temperature change during the heating and the cooling period can respectively be fitted using Eq. 1 and Eq.2 The characteristic thermal time is considered during the cooling phase for several reasons. First, it is harder to measure it during the loading as because the cyclic variations due to the thermo-elastic coupling. Also, the electronic control of the machine is hard to adjust, and the first loading cycles often do not respect the expected signal, which makes more complex the identification of the initial phase of the thermal curve. Hence, we have $\tau_d = \tau_{eq}$. Knowing τ_{eq}, the next step is to solve Eq. 9 for the cyclic loading block which leads to the following expression:

$$\theta(t) = \frac{f_r \tau_{eq} \Delta^*}{\rho c} \times \left(1 - e^{-t/\tau_{eq}}\right) \quad \textit{Eq. 10}$$

22

Finally, the equivalent dissipation per cycle can be written as:

$$\Delta^* = \frac{\rho c \overline{\theta_{MAX}}}{f_r \cdot \tau_{eq}} \qquad \textit{Eq. 11}$$

We haven't identified the heat capacity for the system "rope and water". However, we consider it to be constant and we define Δ' such that:

$$\Delta' = \frac{\Delta^*}{\rho c} \qquad \textit{Eq. 12}$$

This evaluated Δ' can't be seen as the dissipated energy of the rope but only as an evaluation of it considering the effect of the water film both on the temperature measurement and on the solving heat equation. It also means that, for now, the value evaluated cannot be directly compared to the one obtained from the hysteresis curve or computed from a numerical simulation of the rope under tension. This expression enables the heat-build up curve to be plotted, as shown in Figure 20. We observe that the dissipation per cycle increases with the loading range. On the contrary, for small load ranges, the dissipation decreases and is harder to measure precisely. However, at small load ranges, we measure a key parameter for the fatigue at high number of cycles.

Once this curve is generated, the next step is to try to relate it to fatigue properties.

An approach using graphical and empirical analysis of the heat build-up curve has been successfully performed on numerous materials previously [21,24]. It is based on the analysis of the shape of the curve. More precisely, changes in the shape of the curve are related to dissipation mechanism changes and possibly, to fatigue lifetimes at given loads. For some materials, it has been observed empirically that the first change of slope can be efficiently related to a fatigue lifetime of 10^6 cycles [33–35].

The energy criterion chosen enables the number of cycles leading to failure N to be related to the equivalent dissipated energy during the stabilized cycle Δ^*. This relation is written:

$$\Delta^* N^b = C \qquad \textit{Eq. 13}$$

With b and C the model parameters to identify. The energy criterion has been applied with success on metallic material [21], elastomers [24] and composites (Jegou et al., 2013; Navrátil et al., 2020, 2023). The identification of the two parameters requires two equations with known N and Δ^*. A first couple is given by using the fatigue test results at high loads (quickly obtained, short lifetimes) for which the dissipated energy has been measured. The second pair is chosen empirically and is associated with the first change of slope of the heat build-up curve; in this study, we consider that this first change of slope is associated to a lifetime of 10^5 cycles, to be more conservative (see the arrow in Figure 20).

Self-heating prediction

This section is devoted to fatigue lifetime prediction based on a well-defined self-heating curve for 4T sub-ropes. A global dissipation per cycle was measured and calculated on the surface of the sub-rope.

The self-heating curve is presented in Figure 20. The results obtained by three different operators, are superposed to show the repeatability of the measurements.
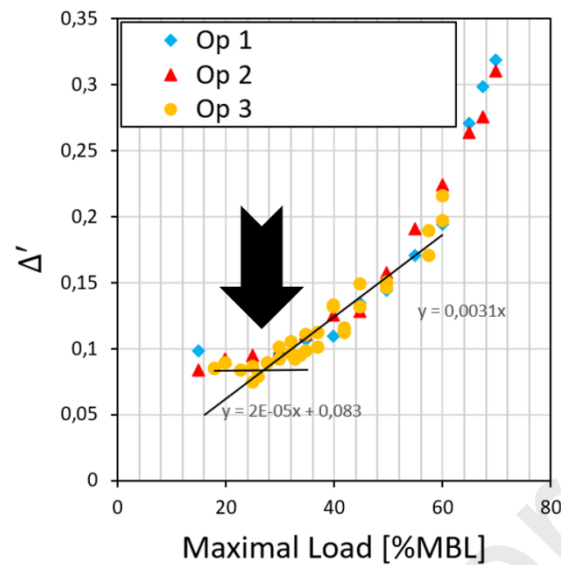
Figure 20 - Heat build-up curve for 4T sub-ropes and linear fit of two regimes (black continue lines). The global dissipation per cycle Δ' is plotted versus the maximal load during a cycle block ; the maximal Results from self-heating tests performed by three operators ("Op 1", "Op 2", "Op 3").

On Figure 20, we can first confirm the good repeatability of this experimental procedure; from the experimental set-up to the data treatment leading to the self-heating curve, obtained by three different operators. Several steps of the procedure can be operator dependent such as the splices which were made by each of the operators; the watering system, which is installed manually, also has an important impact on the infrared-measurement. It is important that each of the operators treats the data following the same method. To conclude, as it is a new experimental protocol, it is important, as a first step, to underline that any operator can perform it and should obtain a similar result.

The self-heating curves obtained provide a precise description of the equivalent dissipation changes before and after 30%MBL. Graphically, the first change of slope (associated to a change of dissipation regime) appears to be at 25%MBL (this graphical analyze is also associated to inaccuracies due to the markers size). As mentioned earlier, in this study, this first change of slope is associated to a lifetime of 10^5 cycles to be more conservative.

This graphical and empirical approach, which involves determining graphically the first change of slope and then relating this change to a fatigue lifetime, would of course deserves a deeper understanding of the dissipative mechanisms. As noted previously, up to five main mechanisms are contributing to the heat-build-up [12]. These are related to the dissipative behaviour of the material and to the friction at several scales within the rope construction. Also, the contact surfaces are changing during a fatigue test (rearrangement of a rope-yarns inside a strand) which induces changes in the friction coefficient. Much more detailed investigations would be required to replace the graphical approach by modelling of the physical mechanisms along the self-heating curve, which would be the best way to analyze the heat build-up curve.

However, we can propose a very efficient prediction using the global dissipated energy per cycle as an energy criterion following Eq. 13. Figure 21 plots the global dissipation per cycle measured versus the maximum load (%MBL) of the fatigue tests. The two stars on the curve are the points used to identify the parameters b and C of the model. The experimental data (circles) correspond to self-heating

24

measurements performed at the beginning of fatigue tests (i.e. not during a self-heating protocol). Hence, these points were not used for the identification of the energy criterion and can be used to validate our model and criterion.
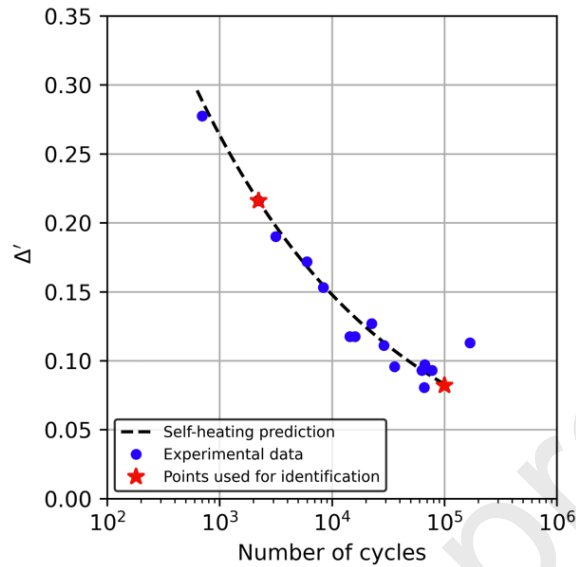
Figure 21 - Equivalent dissipation of the sub-rope and the water versus the number of cycles. Comparison between the model prediction of the energy criterion following Eq. 13 and the measured equivalent dissipation at the beginning of fatigue tests

We observe that the model prediction is in accordance with the experimental measurements. The measurements show a very small dispersion and allows to conclude on the ability of the energetic criterion to predict the number of cycles to failure from the cyclic dissipation obtained using the heat build-up method.

However, it can be complex to perform heat build-up measurement depending on experimental set-up. Hence, for engineering, it is more adapted to have a model that relates the number of cycles to failure to the maximum load. From the relation between the number of cycles and the energy criterion and using a fit of the heat build-up curve with a third-order polynomial, we can obtain a relationship between the equivalent cyclic dissipation energy and the maximal load of a fatigue test and then, associate the appropriate number of cycles to failure for this given load. Hence, it is possible to predict the mean fatigue T-N curve.

Figure 22 presents a comparison between the self-heating prediction (black continue line) and the experimental fatigue curve (circles). As explained previously, the triangle is the fatigue lifetime empirically associated with the first change of slope observed on the self-heating curve as explained previously (Figure 20).

25
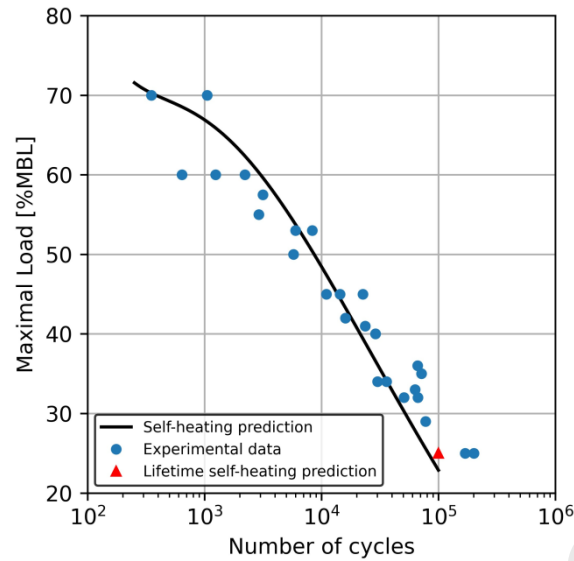
Figure 22 - Predicted fatigue plots using the self-heating prediction method on a 4T sub-rope scale based on the energy criterion (black continuous line and red triangle). Comparison with the experimental T-N curve obtained on a 4T sub-rope scale (blue circles)

The self-heating prediction is in accordance with the experimental results. It is a conservative prediction that may underestimate the lifetime of the sub-rope for longer lifetimes.

This study showed that, using a heat build-up test of a duration of only half a day, we can propose an accurate description of the T-N fatigue curve. This method would allow considerable experimental time savings. To obtain this fatigue curve for a 4T sub-rope, several fatigue test campaigns over 6 years were required. Moreover, the importance of the construction parameters on the fatigue response of the sub-rope was shown. Using the self-heating method could allow the fatigue durability of several construction parameters and of several coatings to be investigated in a much reduced amount of time.

The main objective of future studies is to have a better understanding of the physical mechanisms and to be able to replace the graphical approach. A mesoscopic scale model, at the rope-yarn scale, is being developed to help understand the complex nonlinear dissipative behaviour of polyamide 6 twisted sub-ropes [38,39].

4. Conclusions

A fatigue study on 4T sub-rope samples provided a T-N curve up to 10^5 cycles for 25% MBL. This curve allows to validate the linear trend of the fatigue lifetime in a lin – log scale for the 4T sub-rope sample. This scale is conservative, and this result adds confidence for the use of polyamide as mooring lines.

An investigation of the damage mechanisms was performed. The key observations are that the density of the sub-ropes evolves due to the compaction and radial compression of the rope-yarns inside the strand and that after cycling the rope-yarns become more compact and aligned. The contact surfaces between rope-yarns also change with the loading, due to the change of section of the rope-yarns (from elliptic to prismatic). A damaged area due to the inter-strand friction was observed. The observations also revealed a lustering effect similar to observations made on other types of textile ropes [32]. Hence, a fatigue test changes significantly the 3 main parameters influencing the fatigue lifetime and the mechanical response of the sub-rope, which are: the geometry of contact, the friction coefficient and the organization of the sub-components.

These changes should be considered during the monitoring of in-service mooring lines for offshore floating wind turbines. Hence, further work on the characterization of the changes of the mechanical properties of polyamide 6 ropes with the number of cycles should be performed (such as dynamic stiffness). Fatigue tests with strain monitoring could be an experimental approach to evaluate these mechanical changes. Such work should allow to have better predictions of the mooring system response after significant fatigue loading (for example, after 5 years at-sea) and could be valuable for the use of digital twin models.

The self-heating method was also investigated with the aim of a faster evaluation of the fatigue properties of ropes. A prediction based on a self-heating curve was proposed. This prediction is conservative (it may underestimate the fatigue lifetime for lifetime longer than 10^5 cycles) and is in very good accordance with the fatigue results obtained on the 4T sub-rope. The self-heating method seems to be a powerful solution to avoid the complexity and long testing times required for the fatigue studies on synthetic sub-ropes. It may also be useful in evaluating different constructions and coatings. However, there is a need to extend our understanding of the dissipation mechanisms in order to improve the graphical identification methods.

5. Acknowledgements.

6. References

[1]   Offshore Wind Europe. Wind energy in Europe: 2022 Statistics and the outlook for 2023-2027. 2021.

[2]   Davies P, Chailleux E, Bunsell A, Grosjean F, Francois M. Prediction of the long term behavior of synthetic mooring lines. Days, Houston, Texas: OTC; 2003, p. OTC-15379-MS. https://doi.org/10.4043/15379-MS.

[3]   Flory JF, Banfield SJ, Berryman C. Polyester Mooring Lines on Platforms and MODUs in Deep Water. Days, Houston, Texas, U.S.A.: OTC; 2007, p. OTC-18768-MS. https://doi.org/10.4043/18768-MS.

[4]   Kenney MC, Mandell JF, McGarry FJ. Fatigue behaviour of synthetic fibres, yarns, and ropes. J Mater Sci 1985;20:2045–59. https://doi.org/10.1007/BF01112288.

[5]   Bunsell AR, Hearle JWS. A mechanism of fatigue failure in nylon fibres. J Mater Sci 1971;6:1303–11. https://doi.org/10.1007/BF00552044.

[6]   Colomban Ph, Herrera Ramirez JM, Paquin R, Marcellan A, Bunsell A. Micro-Raman study of the fatigue and fracture behaviour of single PA66 fibres: Comparison with single PET and PP fibres. Eng Fract Mech 2006;73:2463–75. https://doi.org/10.1016/j.engfracmech.2006.04.033.

[7]   Ramirez JMH, Bunsell AR, Colomban Ph. Microstructural mechanisms governing the fatigue failure of polyamide 66 fibres. J Mater Sci 2006;41:7261–71. https://doi.org/10.1007/s10853-006-0421-0.

[8]   Le Clerc C, Monasse B, Bunsell AR. Influence of temperature on fracture initiation in PET and PA66 fibres under cyclic loading. J Mater Sci 2007;42:9276–83. https://doi.org/10.1007/s10853-007-1864-7.

[9]   Lechat C, Bunsell AR, Davies P, Piant A. Mechanical behaviour of polyethylene terephthalate & polyethylene naphthalate fibres under cyclic loading. J Mater Sci 2006;41:1745–56. https://doi.org/10.1007/s10853-006-2372-x.

[10]   Davies P, Bunsell AR, Chailleux E. Tensile fatigue behaviour of PBO fibres. J Mater Sci 2010;45:6395–400. https://doi.org/10.1007/s10853-010-4721-z.

[11]   Herrera-Ramirez J-M. Les mécanismes de fatigue dans les fibres thermoplastiques. Thèse de Doctorat, Ecole Nationale Supérieure des Mines de Paris, 2004.

[12]   Parsey MR. The Fatigue Resistance And Hysteresis Of Man-Made Fibre Ropes, 1983, p. SPE-11908-MS. https://doi.org/10.2118/11908-MS.

[13]   Mandell JF. Modeling of Marine Rope Fatigue Behavior. Text Res J 1987;57:318–30. https://doi.org/10.1177/004051758705700602.

[14]   Seo M, Wu HC, Chen J, Toomey CS, Backer S. Wear and Fatigue of Nylon and Polyester Mooring Lines. Textile Research Journal 1997;67. https://doi.org/10.1177/004051759706700701.

[15]   Bain C, Davies P, Riou L, Marco Y, Bles G, Damblans G. Experimental evaluation of the main parameters influencing friction between polyamide fibers and influence of friction on the abrasion resistance. J Text Inst 2022:1–9. https://doi.org/10.1080/00405000.2022.2105075.

[16]   Banfield S, Ridge IML. Fatigue durability of nylon rope for permanent mooring design. OCEANS 2017 - Aberd., Aberdeen, United Kingdom: IEEE; 2017, p. 1–9. https://doi.org/10.1109/OCEANSE.2017.8084825.

[17]   Chevillotte Y. Characterization of the long-term mechanical behavior and the durability of polyamide mooring ropes for floating wind turbines. Thèse de Doctorat, Université Bretagne Loire, 2020.

[18]   Chevillotte Y, Marco Y, Davies P, Bles G, Arhant M. Fatigue of polyamide mooring ropes for floating wind turbines. MATEC Web Conf 2018;165:10002. https://doi.org/10.1051/matecconf/201816510002.

[19]   Sorum SH, Fonseca N, Kent M, Faria RP. Modelling of Synthetic Fibre Rope Mooring for Floating Offshore Wind Turbines. J Mar Sci Eng 2023;11:193. https://doi.org/10.3390/jmse11010193.

[20]   Rosa GL, Risitano A. Thermographic methodology for rapid determination of the fatigue limit of materials and mechanical components. Int J Fatigue 2000. https://doi.org/10.1016/S0142-1123(99)00088-2.

[21] Doudard C, Calloch S, Cugy P, Galtier A, Hild F. A probabilistic two-scale model for high-cycle fatigue life predictions. Fatigue Fract Eng Mater Struct 2005;28:279–88. https://doi.org/10.1111/j.1460-2695.2005.00854.x.

[22] Jegou L, Marco Y, Le Saux V, Calloch S. Fast prediction of the Wöhler curve from heat build-up measurements on Short Fiber Reinforced Plastic. Int J Fatigue 2013;47:259–67. https://doi.org/10.1016/j.ijfatigue.2012.09.007.

[23] Humeau C, Davies P, LeGac PY, Jacquemin F. Influence of water on the short and long term mechanical behaviour of polyamide 6 (nylon) fibres and yarns. Multiscale Multidiscip Model Exp Des 2018;1:317–27. https://doi.org/10.1007/s41939-018-0036-6.

[24] Marco Y, Masquelier I, Le Saux V, Charrier P. Fast prediction of the wöhler curve from thermal measurement for a wide range of NR and SBR compounds. Rubber Chem Technol 2017;90:487–507. https://doi.org/10.5254/rct.16.83755.

[25] Le Saux V. Celenos users manual, Internal report. ENSTA Bretagne: ENSTA Bretagne; 2017.

[26] Flory JF, Banfield SJ, Ridge IML, Yeats B, Mackay T. Mooring systems for marine energy converters. OCEANS 2016 MTSIEEE 2016:1–13. https://doi.org/10.1109/OCEANS.2016.7761007.

[27] Oland E, Schlanbusch R, Falconer S. Condition Monitoring Technologies for Synthetic Fiber Ropes - a Review. Int J Progn Health Manag 2020;8. https://doi.org/10.36001/ijphm.2017.v8i2.2619.

[28] Davies P, Lacotte N, Kibsgaard G, Craig R, Cannell D, François S, et al. Bend Over Sheave Durability of Fibre Ropes for Deep Sea Handling Operations. Vol. 1 Offshore Technol., Nantes, France: American Society of Mechanical Engineers; 2013, p. V001T01A064. https://doi.org/10.1115/OMAE2013-11332.

[29] Schmieder A, Heinze T, Michael M. Failure Analysis of High Strength Fiber Ropes. Mater Sci Forum 2015;825–826:891–8. https://doi.org/10.4028/www.scientific.net/MSF.825-826.891.

[30] Leech CM. The modelling of friction in polymer fibre ropes. Int J Mech Sci 2002:621–43. https://doi.org/10.1016/S0020-7403(01)00095-9.

[31] Bain C. Compréhension et modélisation des mécanismes de contact des câbles en polyéthylène haut module. Thèse de Doctorat, Université Bretagne Loire, 2020.

[32] Bain C, Marco Y, Davies P, Bles G, Reinhart T, Albouy P-A. An investigation of the appearance of lustering on HMPE fiber ropes. Appl Ocean Res 2022;125:103244. https://doi.org/10.1016/j.apor.2022.103244.

[33] Abello LS, Marco Y, Le Saux V, Robert G, Charrier P. Fast Prediction of the Fatigue Behavior of Short Fiber Reinforced Thermoplastics from Heat Build-up Measurements. Procedia Eng 2013;66:737–45. https://doi.org/10.1016/j.proeng.2013.12.127.

[34] Le Saux V, Marco Y, Calloch S, Doudard C, Charrier P. Fast evaluation of the fatigue lifetime of rubber-like materials based on a heat build-up protocol and micro-tomography measurements. Int J Fatigue 2010;32:1582–90. https://doi.org/10.1016/j.ijfatigue.2010.02.014.

[35] Leveuf L, Marco Y, Le Saux V, Navrátil L, Leclercq S, Olhagaray J. Fast screening of the fatigue properties of thermoplastics reinforced with short carbon fibers based on thermal

measurements. Polym Test 2018;68:19–26. https://doi.org/10.1016/j.polymertesting.2018.03.045.

[36] Navrátil L, Carrere N, Le Saux V, Marco Y, Leclercq S. Influence of thermal diffusion on thermoelastic coupling and dissipated energy fields evaluated in the heterogeneous case of a woven composite. Compos Struct 2023;308:116711. https://doi.org/10.1016/j.compstruct.2023.116711.

[37] Navrátil L, Leveuf L, Le Saux V, Marco Y, Olhagaray J, Leclercq S, et al. A model to describe the cyclic anisotropic mechanical behavior of short fiber-reinforced thermoplastics. Mech Time-Depend Mater 2020;24:481–503. https://doi.org/10.1007/s11043-020-09445-1.

[38] Civier L. Characterization and modelling of the fatigue and durability of polyamide mooring lines for offshore floating wind turbines. Thèse de Doctorat, Université Bretagne Loire, 2023.

[39] Civier L, Bles G, Davies P, Marco Y. FEM Modelling of the Mesoscopic Section of a Polyamide Mooring Subrope for Floating Offshore Wind Turbine; Understand the Friction To Predict the Fatigue Life., 2023. https://doi.org/10.23967/marine.2023.095.

Highlights:

• Extended S-N curve for a wet laboratory scale polyamide 6 sub-rope reaching 10^5 cycles

• Investigation of the damage mechanisms using X-ray tomography analysis and SEM images

• Use of a heat build-up measurement protocol for a rapid evaluation of the fatigue properties of ropes.

Declaration of interests

☒ The authors declare that they have no known competing financial interests or personal relationships that could have appeared to influence the work reported in this paper.

☐ The authors declare the following financial interests/personal relationships which may be considered as potential competing interests: